

ON THE INNER RADIUS EVOLUTION WITH FLUXES OF THE NEUTRON STAR BINARY SERPENS X-1

CHIA-YING CHIANG¹, ROBERT A. MORGAN¹, EDWARD M. CACKETT¹, JON M. MILLER², SUDIP BHATTACHARYYA³, AND TOD E. STROHMAYER⁴

¹Department of Physics and Astronomy, Wayne State University, 666 W. Hancock, Detroit, MI 48202, USA

²Department of Astronomy, The University of Michigan, 500 Church Street, Ann Arbor, MI 48109-1046, USA

³Department of Astronomy and Astrophysics, Tata Institute of Fundamental Research, Mumbai 400005, India and

⁴X-Ray Astrophysics Lab, Astrophysics Science Division, NASA's Goddard Space Flight Center, Greenbelt, MD 20771, USA

Draft version October 8, 2018

ABSTRACT

We analyze the latest *Suzaku* observation of the bright neutron star system Serpens X-1 taken in 2013 October and 2014 April. The observation was taken using the burst mode and only suffered mild pile-up effects. A broad iron line is detected in the X-ray spectrum. We test different models and find that the iron line is asymmetric and best interpreted by relativistic reflection. The relativistically broadened iron line is generally believed to originate from the innermost regions of the accretion disk, where strong gravity causes a series of special and general relativistic effects. The iron line profile indicates an inner radius of $\sim 8 R_G$. The asymmetric iron line has been observed in a number of previous observations, which gives several inner radius measurements at different flux states. We find the inner radius to be consistent over a wide range of luminosity, implying that the inner radius of Serpens X-1 does not evolve significantly over the range of $L/L_{\text{Edd}} \sim 0.2 - 0.6$.

Keywords: neutron star

1. INTRODUCTION

A Low-mass X-ray Binary (LMXB) is a compact system that is composed of a stellar-mass black hole or a neutron star with a low-mass ($\lesssim 1 M_{\odot}$) companion. Both black hole (BH) and neutron star (NS) LMXBs are known to exhibit a number of spectral states, and show different behavior on color-color or hardness-intensity diagrams. Hasinger & van der Klis (1989), using a number of observations taken by the European X-ray Observatory (*EXOSAT*), classified NS LMXBs as two types, “atoll” and “Z” sources, based on their X-ray luminosity, spectral and timing properties. The Z sources show three-branches (horizontal, normal and flaring branches), Z-shaped color-color diagrams and radiate at luminosities close to the Eddington luminosity (L_{EDD}). The atoll sources display fragmented color-color diagrams with the island state appearing isolated from the so-called banana branch, and cover a larger luminosity range. The two classes of sources differ in their spectral and timing properties. The Z sources usually go through their tracks on the color-color diagram in only one day, whereas the atoll sources show state transitions on longer timescales (days to weeks). The X-ray spectra of Z sources are “soft” on all branches, and those of atoll sources are “soft” at high luminosities and “hard” at low luminosities. Lin et al. (2009) studied the outburst and decay of XTE J1701-462 and found the object showed all characteristics of Z and atoll sources when its luminosity decreases from super-Eddington values toward low Eddington fractions. This implies that whether a neutron star is an atoll or a Z is determined by the Eddington fraction.

It is generally believed that a geometrically thin, optically thick accretion disk (Shakura & Sunyaev 1973) is formed around the central source when accreting matter from the companion star. The accretion disk emits thermal emission which can be described as a quasi-blackbody component. Seed photons from the accre-

tion disk can be Compton up-scattered to high energies, which can be approximated as a power-law component. In NS LMXBs, additional high-energy photons coming from the boundary layer originating from the hot flow between the accretion disk and the neutron star surface may be present in the X-ray spectrum as well. High-energy photons from either the Comptonized, power-law component or the boundary layer emission can be absorbed by the accretion disk, and then atomic transitions take place to cause “reflected” fluorescent lines in the X-ray spectrum (Fabian et al. 1989). Reflection coming from the innermost area of the accretion disk is likely shaped by relativistic effects due to strong gravity of the compact central object (Fabian et al. 2000). The most prominent feature in the relativistic reflection spectrum is the skewed Fe K line, which has been widely observed in BH and NS LMXBs. By measuring the shape of the Fe K line, a reliable method to determine the inner radius of the accretion disk has been developed.

During the high-flux, soft states, in which the X-ray spectra of LMXBs are dominated by thermal emission, the accretion disk extends down to the innermost stable circular orbit (ISCO). When sources step down to the hard states, in which a power-law-like, Comptonized component dominates the X-ray spectrum, it is thought that the accretion disk recedes and geometrically thick, optically thin Advection-Dominated Accretion Flows (ADAF) replace the inner accretion disk (Shapiro et al. 1976; Narayan & Yi 1995). The theory suggests that state transitions are results of changes in the innermost extent of the accretion disk and predicts that the accretion disk is truncated during the hard states (see e.g., the review by Done et al. 2007). Nonetheless, relativistically blurred iron lines have been observed in the hard states of both BH (Miller et al. 2006; Reis et al. 2009) and NS LMXBs (Degenaar et al. 2015; Di Salvo et al. 2015), which indicates that the ac-

cretion disk is not truncated in the hard states and leads to challenges for the ADAF scenario. Reis et al. (2010) studied several BH LMXBs in the hard states and found iron emission lines in half of the sample, and detailed analyses on the line profiles exclude a truncated disk in each source. Cackett et al. (2010) analyzed iron lines in a large sample of NS LMXBs and found no obvious dependence of the inner radius on flux, though some sources in the sample were only observed once. Most of the spectral states of LMXBs show a positive correlation between hardness and intensity, but what drives the evolution of color-color/hardness-intensity diagrams is still debated. Probing the evolution of the inner radius is an approach to test theory and helps to better understand transitions between states. In order to tackle this issue, multiple observations at different flux states on a single source are preferred.

Serpens X-1 was classified as an atoll source and observed with all major X-ray missions in the past. In many of the observations relativistic iron lines have been reported (Bhattacharyya & Strohmayer 2007; Cackett et al. 2008, 2010; Miller et al. 2013; Chiang et al. 2015), making it an ideal source for probing the evolution of the inner radius of NS LMXBs. In the present work we analyze the latest and longest *Suzaku* observation, and further study the flux dependence of the inner radius. All spectral fitting was performed using the XSPEC 12.8.2 package (Arnaud 1996) with “wilm” abundances (Wilms et al. 2000). Uncertainties are quoted at 90% of confidence level in this paper if not stated in particular.

2. DATA REDUCTION

Suzaku observed Serpens X-1 during 2013 October 1, 2014 March 13 and April 10 (obs. ID 408033010, 408033020 and 408033030), resulting in ~ 130 ks, ~ 82 ks and ~ 23 ks exposure time (HXD/PIN detector), respectively. The X-ray Imaging Spectrometer (XIS) detectors were operated in burst mode, in order to limit the exposure time per frame and to reduce the effects of pile-up. XIS0 and XIS1 were operated in the 1/4-window mode and 0.135 s frame time, and XIS3 in the full-window mode and 0.1 s frame time. A readout streak is observable in the full-window mode, and can be used to estimate the effect of out of time events in the 1/4-window burst mode observations. Both 3×3 and 5×5 viewing modes were used in these observations. The data were reduced following the *Suzaku* Data Reduction Guide. Since Serpens X-1 is a fairly bright source (> 130 counts s^{-1}), the observation is likely piled-up even in burst mode. We filtered out events that exceed the XIS telemetry limits and proceeded to estimate pile-up effects.

Pile-up effects can be corrected using two methods. We use a concentric circle with a outer radius of $100''$ as the source region. We then extracted a series of source spectra using an annulus with this outer radius, and varying the inner radius. The spectra were fitted using the DISKLINE (Fabian et al. 1989) model in the XSPEC package for simplicity. By comparing the parameters of each spectrum, we found that the spectral shapes and fitting parameters began to settle when the radius of the inner exclusion region is $20''$ – $30''$ or larger, which is consistent with previous observations (Cackett et al. 2010). The other way to do pile-up correction is to use a script

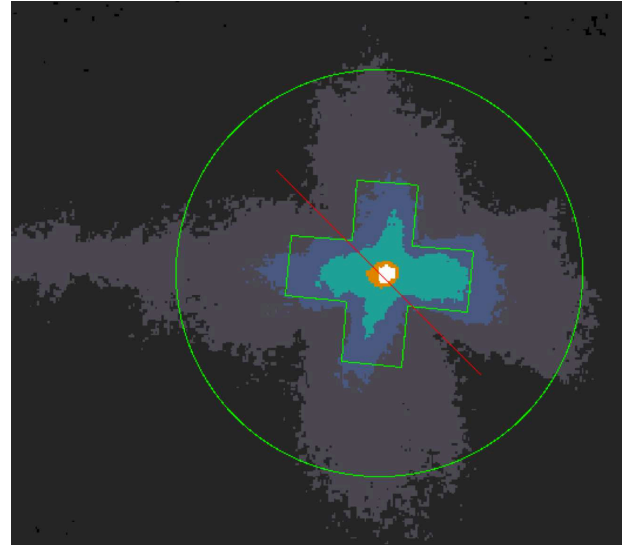


Figure 1. The figures show the source images from the XIS3 detector. The outer green circle is the source region with a radius of $100''$, and the inner plus sign is the exclusion region which is used to correct pile-up effects. A readout streak can be seen on the figure.

in the Interactive Spectral Interpretation System (ISIS) which provides a visual presentation of areas of pile-up in the clean event files¹. Based on the shapes of the areas with a high pile-up fraction (≥ 0.05), we found that the areas affected by pile-up were not circularly-distributed about but rather in the shape of a Maltese cross, which is the shape of the point spread function (PSF) for the telescope. This prompted the use of a plus-sign shaped exclusion region where each side of the polygon is $30''$ in length with right angles (see Figure 1), instead of a circular region, to correct pile-up effects, as a circular exclusion region would filter more photons than actually needed. By comparing the pre-correction and post-correction spectra, we find that pile-up effects in this observation are fairly mild. Pile-up only caused slight differences between ~ 1 – 4 keV and above ~ 7 keV in the spectra and did not affect the iron line profile.

The readout streak was present in the data from XIS3 (see Figure 1), and thus we did not combine the spectrum of XIS3 with that of the other front-illuminated detector, XIS0. We measured the counts taken from a region on the readout streak away from the source and found that on average $\sim 12\%$ of events in the source region were caused by the readout streak in the full-window mode observation, implying $\sim 9\%$ of affected photons in the 1/4-window mode observations.

The Hard X-ray Detector (HXD) was operated as well, in XIS nominal pointing mode, to collect high-energy photons of the source. We reduced the data following standard procedures. The background spectrum was produced by combining the non-X-ray background and the cosmic-X-ray background. As the background dominates above ~ 26.0 keV, we only use the data over the 15.0–26.0 keV energy range in the following analyses. For

¹ http://space.mit.edu/ASC/software/suzaku/pile_estimate.sl

Table 1

Best-fitting parameters for the full continuum which consists of DISKBB, BBODY and power-law components. Parameters of the HXD/PIN spectrum are bound to those of the XIS0 spectrum. The model results in a χ^2/dof of 4521/2409.

Component	Parameter	XIS0	XIS1	XIS3	PIN
Constant		(1.00)	0.96 ± 0.01	1.23 ± 0.02	$0.70^{+0.02}_{-0.01}$
TBABS	N_{H} (10^{22} cm^{-2})	0.97 ± 0.06
	kT_{disk} (keV)	1.36 ± 0.01
DISKBB	N_{disk}	71 ± 3	66^{+3}_{-4}	73^{+3}_{-4}	...
	kT_{bb} (keV)	$2.29^{+0.02}_{-0.01}$
BBODY	N_{bb} (10^{-2})	3.4 ± 0.1	3.1 ± 0.1	3.1 ± 0.1	...
	Γ	$3.61^{+0.21}_{-0.25}$
POWERLAW	N_{pow}	$0.88^{+0.15}_{-0.14}$

both XIS and HXD/PIN detectors, we used the ADDAS-CASPEC tool to combine the spectrum from each observation and obtained a total spectrum for each detector.

3. DATA ANALYSIS

3.1. Continuum Model

Serpens X-1 has been observed by different instruments at different times. There are several continuum models used in previous work. A “full” continuum consisting of a disk blackbody, a blackbody and a power-law components was most used, especially in broadband observations (2006 *Suzaku* observation: Cackett et al. 2008, 2010; 2013 *NuSTAR* observation: Miller et al. 2013). Continuum models including only a disk blackbody and a blackbody, or a blackbody and a power-law were used in previous observations as well, but only in observations with limited energy ranges (Bhattacharyya & Strohmayer 2007; Chiang et al. 2015). We then test the continuum models which successfully fit the archival data on our latest *Suzaku* observation.

We use the XIS data over the 1.0-10.0 keV energy band, and the PIN spectrum over 15.0-26.0 keV. The 1.45 keV-2.5 keV in the XIS spectra were ignored due to poor calibration around the Si and Au edges. An iron K emission line is detected in the spectra. In order not to bias continuum measurements, we first excluded the 5.0-7.5 keV energy band (the iron line band) to test various continuum models in the initial fits. The Galactic absorption is modeled using TBABS in XSPEC; the accretion disk emission is modeled with DISKBB; the blackbody component which is likely caused by the boundary layer is accounted for using BBODY. We added a constant between the spectra (with that of the XIS0 spectrum frozen at 1.00) and linked all parameters except normalizations of DISKBB and BBODY. As there are mild spectral differences between the spectra of different XIS detectors, which are caused by calibration and different observation modes, the normalizations of DISKBB and BBODY components are free to vary for better results. The full continuum results in a $\chi^2/\text{d.o.f.}$ of 4521/2409, with a $\Delta\chi^2 \sim 1060$ lower than the second best model with two lower degree of freedom (d.o.f.). The result is consistent with previous work using broadband X-ray data, implying that the full continuum is the best continuum model. We also test thermal Comptonization model using NTHCOMP (Zdziarski et al. 1996; Źycki et al. 1999) in XSPEC, and it does not improve the fit. Since the full continuum fits significantly better than other continuum

models, we use the full continuum in all following analyses.

The best-fitting parameters of the full continuum are listed in Table 1. It can be seen that the neutral absorption column density N_{H} is higher than any value previously reported. The highest N_{H} obtained from past work was $(7.5 \pm 0.2) \times 10^{-21} \text{ cm}^{-2}$ (1σ uncertainty) obtained from previous *Suzaku* observation (Cackett et al. 2010), while here $(9.7 \pm 0.6) \times 10^{-21} \text{ cm}^{-2}$ is required to fit the data. The value of N_{H} reported in previous literature spans a wide range around $\sim 3\text{-}7.5 \times 10^{-21} \text{ cm}^{-2}$ (Cackett et al. 2008, 2010; Ng et al. 2010), and those obtained from *Suzaku* data are higher than the others. N_{H} is a continuum-dependent parameter which is affected by the low-energy band (Reis et al. 2012). A change in the continuum model may result in a different N_{H} . Given that the best-fitting temperature of the DISKBB component here (1.36 ± 0.01 keV) is slightly higher than that obtained from the previous *Suzaku* observation (1.26 ± 0.01 keV), it is likely that the mild difference below the < 2 keV band can cause a slightly different N_{H} . A well-known calibration issue for the *Suzaku* XIS is the presence of contamination (mostly diethylhexyl phthalate or DEHP) in the optical path. The level of contaminant, has changed over the mission lifetime and does affect the observed N_{H} . While corrections to model the contamination are included in the CALDB, this could likely explain the change in N_{H} we observe here. Moreover, the latest *Suzaku* observation has a significant longer exposure time than the previous one and thus collects much more photons in the low-energy band, which may lead to the need of high N_{H} as well. Note that the constant for the XIS3 is 1.23 ± 0.02 . In previous section we found that the effect caused by the readout streak is $\sim 9\%$. The constant is still slightly higher than expected when the effect is accounted for due to unknown reason. The best-fitting values of remaining parameters shown in Table 1 are consistent with Cackett et al. (2008).

3.2. Phenomenological Models

We then included the 5.0-7.5 keV data and added a Gaussian component on top of the continuum to model the broadband X-ray spectrum with the iron emission line. We restricted the energy of the Gaussian line to be 6.4-6.97 keV, which is the energy range that the Fe K α line can appear in the spectrum. The fitting results are listed in Table 2. The absorption column density is slightly higher than the value of continuum fitting. The photon index Γ tends to be higher than those previously

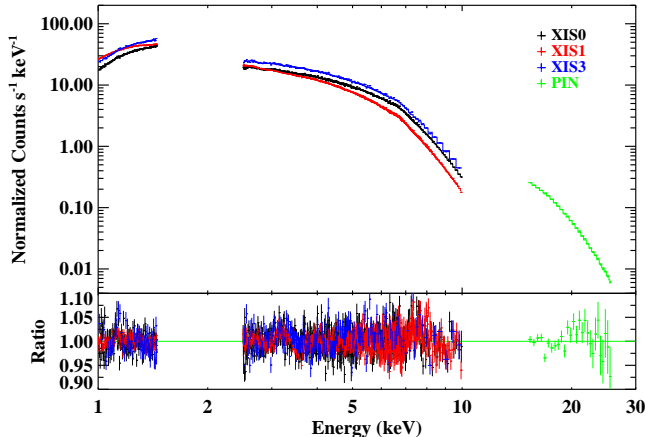


Figure 2. The figure shows the XIS0 (black), XIS1 (red), XIS3 (blue) and PIN (green) spectra of Serpens X-1 fitted with the full continuum plus a DISKLINE component. The lower panel is the data/model ratio, and it can be seen that the model fits the broadband spectrum well.

reported. Note that the Gaussian width $\sigma = 0.83 \pm 0.04$ keV is higher than the broadest value in published literature ($\sigma = 0.61$ keV, see Cackett et al. 2012), indicating the existence of a broad Fe K line. In addition, the equivalent width (EW) of the line 197^{+16}_{-14} eV is larger than values obtained from previous Serpens X-1 observations (Bhattacharyya & Strohmayer 2007; Cackett et al. 2008, 2010; Chiang et al. 2015). These may imply that the Gaussian component is fitting part of the continuum, and whether the Fe K line is symmetric or not should be further investigated.

We replaced the Gaussian component with the DISKLINE model to fit the spectrum in order to examine if the line profile is better interpreted by relativistic effects. It is generally believed that the Fe K line originating from an accretion disk around objects of strong gravity (i.e., black holes or neutron stars) may be shaped by a series of relativistic effects, including relativistic beaming and gravitational redshift, and appear to be broad and asymmetric. We froze the outer disk radius R_{out} at $1000 R_{\text{G}}$ in the fitting with other parameters of DISKLINE free to vary. As shown in Table 2, the fit improves by $\Delta\chi^2 = 54$ with two lower degrees of freedom compared to the Gaussian model, and the model fits the data well (see Fig. 2). The F-test probability is $\sim 3.59 \times 10^{-7}$, which is convincing that the DISKLINE model explains the data better. The EW of the Fe line obtained via the DISKLINE model is 134^{+5}_{-13} eV, which is also consistent with previous results (Cackett et al. 2008; Chiang et al. 2015).

The temperatures of the DISKBB and BBODY components are nearly identical in both models. Although the photon indices Γ obtained from the models seem to be different, the fluxes of the powerlaw component are quite similar. The differences between Γ may be led by the mild differences in the blackbody temperatures. The DISKLINE model gives a slightly lower N_{H} , indicating the result may be mildly model-dependent.

The parameters of the DISKLINE component are remarkably similar to previously reported numbers

Table 2

The table lists the results of phenomenological models. For simplicity, we only present results of XIS1 (the $\chi^2/\text{d.o.f.}$ is of the entire data set). The constant of each spectrum remains the same as those displayed in Table 1.

Component	Parameter	Gaussian	DISKLINE
TBABS	N_{H} (10^{22} cm^{-2})	$1.08^{+0.03}_{-0.05}$	$0.89^{+0.08}_{-0.04}$
DISKBB	kT_{disk} (keV)	1.36 ± 0.01	1.36 ± 0.01
	N_{disk}	74 ± 3	68^{+3}_{-2}
BBODY	kT_{bb} (keV)	$2.31^{+0.02}_{-0.01}$	$2.26^{+0.03}_{-0.04}$
	N_{bb} (10^{-2})	3.3 ± 0.1	3.4 ± 0.1
POWERLAW	Γ	$3.98^{+0.14}_{-0.16}$	$3.27^{+0.31}_{-0.20}$
	N_{pow}	$1.16^{+0.14}_{-0.13}$	$0.71^{+0.16}_{-0.10}$
Gaussian	E_{line}	$6.4^{+0.01}_{-0.01}$...
	σ (keV)	0.83 ± 0.04	...
	N_{gau} (10^{-3})	9.6 ± 0.6	...
DISKLINE	E_{line} (keV)	...	$6.97^{+0.01}_{-0.01}$
	β	...	-4.49 ± 0.20
	R_{in} (GM/c^2)	...	$8.0^{+0.3}_{-0.2}$
	i (deg)	...	23 ± 1
	N_{diskline} (10^{-3})	...	$6.1^{+0.4}_{-0.3}$
	EW (eV)	197^{+16}_{-14}	134^{+5}_{-13}
	$\chi^2/\text{d.o.f.}$	6661/3438	6607/3436

(Cackett et al. 2010; Chiang et al. 2015). We obtained an inner radius $R_{\text{in}} = 8.0^{+0.3}_{-0.2} R_{\text{G}}$, which is fairly close to a number of previous results (Cackett et al. 2012; Miller et al. 2013; Chiang et al. 2015), and the line profile is similar as well (see Fig. 3). We also tried to replace the DISKLINE model with the LAOR model, and find that an inner radius of $\sim 8.0 R_{\text{G}}$ is still the best-fitting value. A low inclination angle $i \sim 23 \pm 1$ is required to fit the data, which is expected as low inclination has been reported in a series of past work (Cackett et al. 2010, 2012; Miller et al. 2013; Chiang et al. 2015). Optical observations of Serpens X-1 also point to a low inclination (Cornelisse et al. 2013).

We model all main features shown in the spectrum but still obtain a large $\chi^2/\text{d.o.f.}$, which is likely due to some features that do not seem to have physical origins. Part of the residuals come from the unknown emission feature around 3 keV, which match with a mild change in the effective area. If modeling the feature using a Gaussian component, this yields a better fit of $\Delta\chi^2 = 231$ with three lower degrees of freedom compared to the DISKLINE model. Other residuals are mainly due to random noise in the spectrum, which appear as narrow absorption/emission features but each of them is only seen on the spectrum of a single detector.

3.3. Reflection Model

We learn from the tests of phenomenological models that the iron line is better explained by relativistic reflection. In order to confirm this scenario, we replace the DISKLINE component with a self-consistent reflection model which includes a broadband continuum and all emission lines originated from an illuminated accretion disk. Since the blackbody emission dominates the flux above 10 keV which implies the illuminating source is the boundary layer emission, we use the BBREFL (Ballantyne 2004) grid, which calculates reflected emission from an accretion disk illuminated by a blackbody component, to model the reflection. We use the convolution kernel KDBLUR to account for relativistic effects.

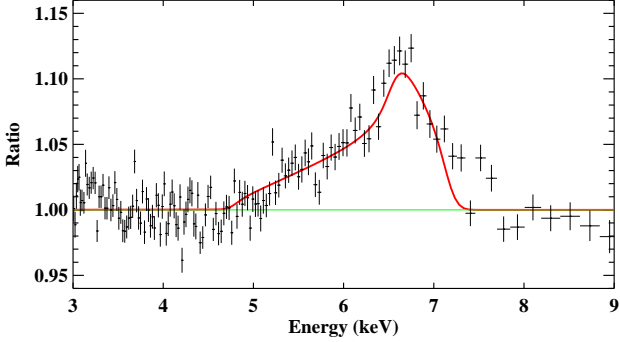


Figure 3. The figure shows the iron line profile (XIS0 data only) fitted with the DISKLINE model.

Table 3

The table lists the results of the reflection. For simplicity, we only present results of XIS1 (the $\chi^2/\text{d.o.f.}$ is of the entire data set though). The constant of each spectrum remains the same as those displayed in Table 1.

Component	Parameter	BBREFL
TBABS	N_{H} (10^{22} cm^{-2})	1.11 ± 0.05
DISKBB	kT_{disk} (keV)	$1.30^{+0.01}_{-0.02}$
	N_{disk}	87^{+4}_{-3}
BBODY	kT_{bb} (keV)	2.32 ± 0.01
	N_{bb} (10^{-2})	3.1 ± 0.1
POWERLAW	Γ	$4.18^{+0.15}_{-0.17}$
	N_{pow}	$1.24^{+0.15}_{-0.20}$
KDBLUR	q	$3.7^{+0.4}_{-0.1}$
	R_{in} (GM/c^2)	$8.2^{+1.4}_{-0.1}$
	i (deg)	26 ± 1
BBREFL	$\log \xi$	$2.75^{+0.10}_{-0.09}$
	N_{bbrefl} (10^{-26})	$2.6^{+1.0}_{-0.5}$
$\chi^2/\text{d.o.f.}$		6487/3436

We list best-fitting parameters in Table 3. It can be seen that the fit has been improved by $\Delta\chi^2 = 120$ compared to the DISKLINE model. The decomposed model and data/model ratio can be found in Fig. 4. We again obtain an inner radius of $\sim 8 R_{\text{G}}$, indicating the measurement is robust. All other parameters are fairly similar with results of those obtained using phenomenological models (see section 3.2).

4. DISCUSSION

Serpens X-1 has been observed by different missions in the past, and there are several measurements on the inner radius which can be found in the literature. As these archival observations were taken at different times, and possibly in different flux states, these offer the possibility to probe the evolution of the inner radius in Serpens X-1. We then check previous work to find fluxes and inner radii obtained from other observations, and compare these numbers with those of the present work. The 0.5–25.0 keV absorption-corrected (unabsorbed) fluxes were converted into luminosities using a distance of 7.7 kpc (from X-ray burst properties, see e.g. Galloway et al. 2008). We list the 0.5–25.0 keV luminosity and inner radius quoted from a number of previous observations (see Table 4). Note that these numbers were calculated using phenomenological models in which the DISKLINE model

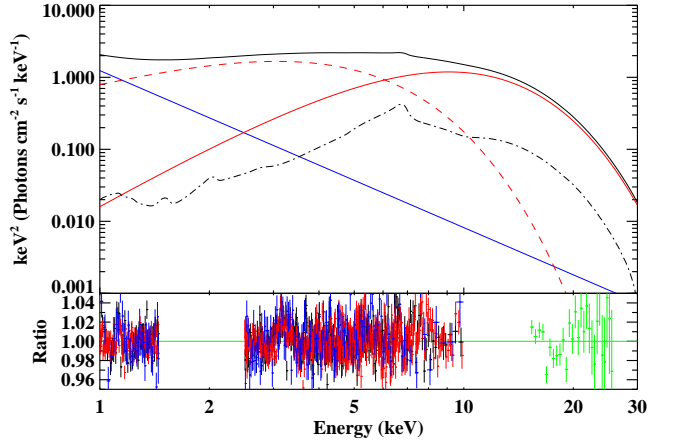


Figure 4. The upper panel shows the decomposed best-fitting model. The red dash line represents the DISKBB component, the red solid line the BBODY component, the blue solid line the POWERLAW component, and the black dot dash line the blurred reflection continuum KDBLUR \times BBREFL. The black solid line on top is the total model with all the components combined. The lower panel shows the data/model ratio, in which black, red, blue, and green data points stand for XIS0, XIS1, XIS3, and PIN data, respectively.

was used to model the iron line. In some references, measurements based on self-consistent relativistic reflection models are also listed, and we find most the results are consistent with phenomenological model calculations. In Cackett et al. (2010) and Miller et al. (2013) a full continuum model which is the same with that of the present work was used, while in Chiang et al. (2015) a continuum model composed of a blackbody and a powerlaw components was used, but the authors reported that the line parameters are not continuum-dependent in that observation.

In order to see how the inner radius evolves with the flux more clearly, we plot the results of Table 4 in Fig. 5. The inner radius spans a range between ~ 8 – $25 R_{\text{G}}$ and the flux between $\sim (3$ – $11) \times 10^{37} \text{ erg s}^{-1}$ (~ 0.2 – 0.6 Eddington ratio L/L_{Edd} if assuming a mass of $1.4 M_{\odot}$). Although some of the 2004 *XMM-Newton* observations give large inner radii of more than $\sim 25 R_{\text{G}}$, these measurements are not well-constrained. Note that the *XMM* data are the least reliable among these archival data due to short exposure and calibration issues of EPIC-PN timing mode data (see e.g. Walton et al. 2012), though the broad line does not seem to suffer from pile-up effects (Miller et al. 2010). In Fig. 5 we treat *XMM* measurements as upper limits. The weighted mean of all inner radius measurements is $\sim 7.9 R_{\text{G}}$, indicating that the inner radius basically does not evolve dramatically with flux. At least it can be seen in Fig. 5 that more constrained measurements of the inner radius fall at a similar value, implying that the accretion disk is not truncated at a large radius at low fluxes. Furthermore, from Fig. 5 it seems that the inner radius does not show flux dependence.

Steiner et al. (2010) found values of the inner radius of the black hole binary LMC X-3 to be consistent within 4–6% across eight X-ray missions, implying the inner radius is stable over different flux states. In neutron

Table 4

The table lists the luminosity and inner radius R_{in} of each previous Serpens X-1 observation. The luminosity was calculated based on the 0.5-25.0 keV absorption-corrected flux (measured using a phenomenological model) and a distance of 7.7 kpc. Luminosities quoted in Cackett et al. (2010) have much larger uncertainties due to including 25% of error on distance. In this work we only compare results of the same source, and uncertainties on distance were excluded. *Note that the flux of the *NuSTAR* observation was measured using the 0.5-40.0 keV band. Since the high-energy tail of this source is weak, the 25.0-40.0 keV energy band only contributes little flux.

Observation	Luminosity (erg/s)	L/L_{Edd}	Inner Radius R_{in} (R_{G})	reference
<i>Suzaku</i> (2006)	$(8.5 \pm 0.1) \times 10^{37}$	0.48	8 ± 0.3	Cackett et al. (2010)
<i>XMM</i> (2004, Obs ID 0084020401)	$(5.0 \pm 0.1) \times 10^{37}$	0.28	25 ± 8	Cackett et al. (2010)
<i>XMM</i> (2004, Obs ID 0084020501)	$(3.6 \pm 0.1) \times 10^{37}$	0.20	14 ± 1	Cackett et al. (2010)
<i>XMM</i> (2004, Obs ID 0084020601)	$(4.6 \pm 0.1) \times 10^{37}$	0.26	26 ± 8	Cackett et al. (2010)
<i>NuSTAR</i> (2013)	$1.1 \times 10^{38}^*$	0.62	10.6 ± 0.6	Miller et al. (2013)
<i>Chandra</i> (2014)	$(6.7 \pm 0.1) \times 10^{37}$	0.38	7.7 ± 0.1	Chiang et al. (2015)
<i>Suzaku</i> (2013-14)	$(7.0 \pm 0.4) \times 10^{37}$	0.40	$8.0^{+0.3}_{-0.2}$	present work

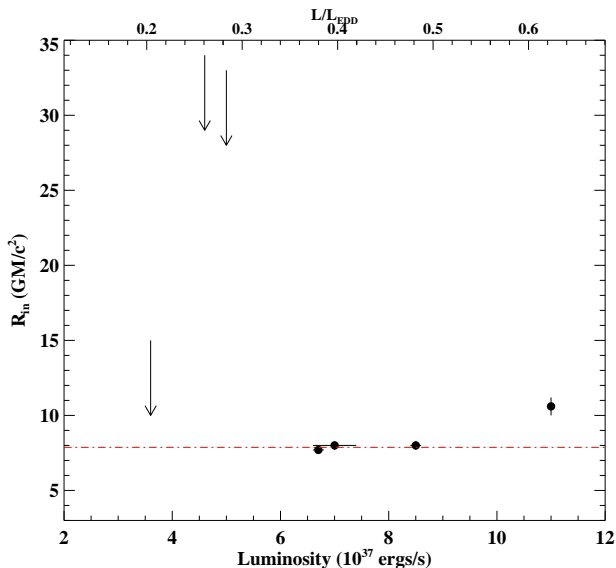


Figure 5. The figure is the visualization of Table 4 shows the inner radii measured in previous literature in different flux states. We assume a mass of $1.4M_{\odot}$ to convert the luminosity into the Eddington ratio L/L_{Edd} . The red dash line marks the weighted mean of the inner radius measurements.

star LMXBs the evolution of inner radius has also been studied. Lin et al. (2010) found that the accretion disk of the neutron star system 4U 1705-44 is close to the neutron star during soft states based on the discovery of the broad iron line. In hard states of 4U 1705-44, whether the accretion disk is truncated is however debated. D'Aì et al. (2010) suggested the accretion disk to be truncated, while Di Salvo et al. (2015) indicated that it is not, down to $\sim 3\%$ of Eddington luminosity. Serpens X-1 has only been observed during soft states, and the inner radius evolution during hard states remains unclear. But in soft states the inner radius is roughly constant over fluxes changing by a factor of around 3.

5. CONCLUSION

We present detailed spectral analysis of the latest, longest *Suzaku* observation of the neutron star LMXB Serpens X-1 in this work. The continuum is best explained by the combination of a disk blackbody component, a single-temperature blackbody component and a powerlaw component, which is consistent with the results of previous broadband observations. We find that the relativistic reflection scenario is the better interpretation of

the iron line profile shown in this observation. The line parameters obtained are pretty similar to a number of previous work. By comparing the inner radius obtained from different observations taken at different flux states, we find no strong evidence that the inner radius is truncated at a large radius when the Eddington ratio is low, though the signal-to-noise ratio is lowest there and the best-fitting values do give large R_{in} even with larger error bars. The comparison shows that inner radius does not evolve dramatically with fluxes. Results of current data indicate that the inner radius stays unchanged at soft states. To further confirm if this stands true for hard states, multiple observations at different times on the same source should be made to cover a wider range of flux states.

This work was greatly expedited thanks to the help of Jeremy Sanders in optimizing the various convolution models. C.Y.C. and E.M.C. gratefully acknowledge support provided by NASA through Chandra Award Number GO4-15041X issued by the Chandra X-ray Observatory Center, which is operated by the Smithsonian Astrophysical Observatory for and on behalf of NASA under contract NAS8-03060. R.M. acknowledges support from the NSF through a Research Experience for Undergraduates program at Wayne State University (NSF grant number PHY1460853).

REFERENCES

- Arnaud, K. A. 1996, in Astronomical Society of the Pacific Conference Series, Vol. 101, Astronomical Data Analysis Software and Systems V, ed. G. H. Jacoby & J. Barnes, 17
- Ballantyne, D. R. 2004, MNRAS, 351, 57
- Bhattacharyya, S., & Strohmayer, T. E. 2007, ApJL, 664, L103
- Cackett, E. M., Miller, J. M., Reis, R. C., Fabian, A. C., & Barret, D. 2012, ApJ, 755, 27
- Cackett, E. M., Miller, J. M., Bhattacharyya, S., et al. 2008, ApJ, 674, 415
- Cackett, E. M., Miller, J. M., Ballantyne, D. R., et al. 2010, ApJ, 720, 205
- Chiang, C.-Y., Cackett, E. M., Miller, J. M., et al. 2015, ArXiv e-prints, arXiv:1509.02969
- Cornelisse, R., Casares, J., Charles, P. A., & Steeghs, D. 2013, MNRAS, 432, 1361
- D'Aì, A., di Salvo, T., Ballantyne, D., et al. 2010, A&A, 516, A36
- Degenaar, N., Miller, J. M., Chakrabarty, D., et al. 2015, MNRAS, 451, L85
- Di Salvo, T., Iaria, R., Matranga, M., et al. 2015, MNRAS, 449, 2794
- Done, C., Gierliński, M., & Kubota, A. 2007, A&A Rev., 15, 1
- Fabian, A. C., Iwasawa, K., Reynolds, C. S., & Young, A. J. 2000, PASP, 112, 1145

Fabian, A. C., Rees, M. J., Stella, L., & White, N. E. 1989, MNRAS, 238, 729

Galloway, D. K., Muno, M. P., Hartman, J. M., Psaltis, D., & Chakrabarty, D. 2008, ApJS, 179, 360

Hasinger, G., & van der Klis, M. 1989, A&A, 225, 79

Lin, D., Remillard, R. A., & Homan, J. 2009, ApJ, 696, 1257

—. 2010, ApJ, 719, 1350

Miller, J. M., Homan, J., & Miniutti, G. 2006, ApJL, 652, L113

Miller, J. M., D'Aì, A., Bautz, M. W., et al. 2010, ApJ, 724, 1441

Miller, J. M., Parker, M. L., Fuerst, F., et al. 2013, ApJL, 779, L2

Narayan, R., & Yi, I. 1995, ApJ, 452, 710

Ng, C., Díaz Trigo, M., Cadolle Bel, M., & Migliari, S. 2010, A&A, 522, A96

Reis, R. C., Fabian, A. C., & Miller, J. M. 2010, MNRAS, 402, 836

Reis, R. C., Fabian, A. C., Ross, R. R., & Miller, J. M. 2009, MNRAS, 395, 1257

Reis, R. C., Miller, J. M., Reynolds, M. T., Fabian, A. C., & Walton, D. J. 2012, ApJ, 751, 34

Shakura, N. I., & Sunyaev, R. A. 1973, A&A, 24, 337

Shapiro, S. L., Lightman, A. P., & Eardley, D. M. 1976, ApJ, 204, 187

Steiner, J. F., McClintock, J. E., Remillard, R. A., et al. 2010, ApJL, 718, L117

Walton, D. J., Reis, R. C., Cackett, E. M., Fabian, A. C., & Miller, J. M. 2012, MNRAS, 422, 2510

Wilms, J., Allen, A., & McCray, R. 2000, ApJ, 542, 914

Zdziarski, A. A., Johnson, W. N., & Magdziarz, P. 1996, MNRAS, 283, 193

Życki, P. T., Done, C., & Smith, D. A. 1999, MNRAS, 309, 561